A&A 421, 295–303 (2004)
DOI: 10.1051/0004-6361:20034193

Astronomy & Astrophysics

An atmospheric model for UZ Librae from mean Hα-line profiles

M. Zboril[1], K. G. Strassmeier[1,⋆], and E. H. Avrett[2]

[1] Astrophysikalisches Institut Potsdam (AIP), An der Sternwarte 16, 14482, Germany
e-mail: kstrassmeier@aip.de
[2] SAO, Harvard-Smithsonian Center for Astrophysics, 60 Garden Street, MA 02138, USA
e-mail: avrett@cfa.harvard.edu

Received 14 August 2003 / Accepted 25 March 2004

Abstract. We present the results from fitting a semi-empirical atmospheric model including a chromosphere and a transition region to the mean (seasonal) Balmer Hα line profiles of the RS CVn-type K0-giant UZ Librae. As a first step, a static 1D spherical model was applied to the mean component of the Hα-emission core and its profile. The main result of the fitting is that the transition region begins at a log mass depth of -1.8 g cm^{-2} at a temperature of 7400 K (approximately 3000 K warmer than the photosphere) and then has a steep increase to the peak temperature of $\approx 10^6$ K. A stellar model in plane-parallel mode with "partial-frequency redistribution" option in the line transfer gave roughly the best fit. Subsequently, two-Gaussian fitting of the phase-dependent Hα-line profiles yields a complex velocity field. The radial velocities, from both the absorption reversal and the main emission component, display rotational and/or orbital modulation. The largest differences between consecutive line profiles occur mostly in the red line wings, suggesting the existence of both an inward-pointed velocity field and sporadic radiation events possibly related to flares. The total Hα emission, as derived from the equivalent width, possibly also displays rotational modulation. Indirect evidence is presented for the existence of circumstellar matter in form of an Hα absorption shell. Finally, a preliminary elemental abundance analysis suggests sub-solar metallicity of [M/H] ≈ -0.5 dex based on ATLAS models, or -0.7 dex based on PHOENIX models.

Key words. stars: late-type – stars: activity – stars: atmospheres – stars: chromospheres – stars: individual: UZ Lib

1. Introduction

The atmospheres of magnetically-active cool stars are known to exhibit most, if not all, features of the active Sun. Firstly, these atmospheres seem to consist also of a photosphere, a chromosphere, and an outer corona with its respective and distinct spectral fingerprints. Secondly, a variety of magnetic activity tracers are observed on such stars, e.g. cool spots, flares, and hot plages (see the recent review by Schrijver 2002). These are usually observed on a much enhanced flux and geometric scale compared to the Sun but are thought to be associated with similar events like rising magnetic-flux tubes, enhanced ultraviolet emission due to coronal heating and long-term light variability due to magnetic cycles.

One of the pioneering atmospheric models for the Sun was that of Vernazza et al. (1973), also known as the VAL atmospheres, which was a one-component description of the solar atmosphere including its photosphere, a chromosphere and a chromosphere-corona transition zone. The structure of the chromosphere was examined further in the subsequent paper by Vernazza et al. (1981). Later on, a number of studies, both with a semi-empirical and a modelling approach, appeared on M-dwarf stars to explain the complex emission-line profiles of its hydrogen Balmer and Ca II H and K transitions (e.g. Giampapa et al. 1982; Houdebine & Panagi 1990; see the review by Houdebine 1996 and references therein). Among the more recent studies is the paper on the active subgiant II Peg by Short et al. (1998). Further improvements to the VAL models have been given by Fontenla et al. (2000, and references therein).

The target in the present paper is UZ Librae (K0III, $P_{\rm rot}$ = 4.77 days), which is the rapidly-rotating primary component of one of the most active RS CVn binaries in the sky. Table 1 summarizes its basic stellar parameters. The star displays photometric variability with an amplitude of up to $0\overset{\rm m}{.}35$ in V due to cool starspots and a long-term trend with an amplitude of, so far, $0\overset{\rm m}{.}5$ (Oláh et al. 2002a) possibly due to a magnetic cycle. In one of the first papers on this star, Grewing et al. (1989) presented IUE spectra to discover an ultraviolet excess which they attributed to a companion star with the effective

Send offprint requests to: M. Zboril, e-mail: mzboril@aip.de

⋆ Visiting Astronomer, Kitt Peak National Observatory, operated by the Association of Universities for Research in Astronomy, Inc. under contract with the National Science Foundation.

Table 1. Basic astrophysical data for UZ Librae.

Parameter	Value	Ref.
Classification	K0III	1
Period, $P_{\rm rot} = P_{\rm orb.}$	4.768241 d	2, 3
Rotational broadening, $v \sin i$	67 km s^{-1}	2, 3
Temperature	4800 K	3
Gravity, $\log g$	2.5	2
Inclination, i	50	4
Metallicity [M/H]/[M/H]$_\odot$	≈−0.6	this paper

1. Bopp & Stencel (1981), 2. Strassmeier (1996), 3. Fekel et al. (1999), 4. Oláh et al. (2002b).

temperature $T_{\rm eff} \approx 8000$ K and $R \approx 1\ R_\odot$. Oláh et al. (2002a) rediscussed the absolute dimensions of the system and concluded that the secondary is most-likely a low-mass cool star and that the ultraviolet excess can be explained by the active chromosphere of the primary. Further references regarding the literature history of the star are summarized in Strassmeier (1996). A detailed spectroscopic analysis by Oláh et al. (2002b), with new Doppler images from the years 1994, 1996, 1997, 1998 and 2000, suggested the presence of two spots 180° apart at low latitudes that remained observable over at least seven years. A polar spot with several appendages was also detected and used to trace the migration rate at high latitudes. Although no clear detection of differential rotation was claimed by Oláh et al. (2002b), they presented evidence that it would be most likely anti solar. In a recent attempt to quantify this result, Oláh et al. (2003) carried out a detailed Fourier analysis of the UZ Lib photometry and detected not only a very precise equatorial rotational period but also the rotation period due to the polar appendages, and thus verified that UZ Lib indeed shows weak anti-solar differential rotation.

In the present paper, we focus our analysis on the physical parameters of the chromosphere and the transition region of UZ Librae. The study is based on high-resolution Hα line profiles from the years 1996, 1997, 1998 and 2000 that were taken simultaneously with the photospheric Doppler images presented earlier by Oláh et al. (2002b). This represents the first attempt to estimate the atmospheric properties of this K0 giant in both the vertical and the azimuthal direction, and to link it to a possibly systematic dynamical behavior.

2. Observations 1996–2000

A total of 56 spectra were obtained with the 0.9 m coudé-feed telescope at Kitt Peak National Observatory (KPNO) between 1996–2000. The same spectra were already used for the Doppler-imaging analysis by Oláh et al. (2002b) and all phases quoted in present paper were computed with their ephemeris. A detailed summary of the detectors, instrumental set-ups and the data-reduction procedure was given in that paper and is not repeated here. Briefly, the observations have a resolution between $R = 27\,000$ to $38\,000$, covering the wavelengths from around 638−675 nm and have typical signal to noise ratios of 200:1.

Figure 1 shows the phase-resolved Hα line profiles for six observing runs in four years (overall Fig. 1); April−May 2000, April 1998, April 1997 and January 1996. Visual inspection of the profile shape already indicates strong variability, sometimes changing from pure emission to strong absorption within a few tenth of a phase. Nevertheless, the seasonally averaged profiles appear very similar from year to year and are the subject of our radiative modelling analysis.

3. The Hα-emission line profile

The seasonally average profiles were computed with equal weights for the individual spectra and centered on the Hα vacuum rest wavelength. However, each individual profile was then fitted with two Gaussians to obtain parameters such as centroid radial velocity, full width half maximum (*FWHM*), and the blue-to-red line-wing asymmetry. The line equivalent widths were calculated from a numerical integration of the observed profile. Figure 2 (left) displays typical two-Gaussian fits for three phases in 1996, while Fig. 2 (right) shows the phase dependency of the residual radial velocity from the main emission component. Figure 3 (left) directly compares the four seasonal mean Hα profiles while the accompanying Fig. 3 (right) shows the equivalent-width variations for the individual profiles for all data. The numerical values of the two-Gaussian fits are listed in Table 2 where λ stands for central wavelength, *FWHM* for the full-width of half-maximum, and W for the equivalent width.

Note that the line broadening of the hydrogen emission profile exceeds the rotational broadening $v \sin i$ by a factor of 1.5, while the width of the absorption reversal is in agreement with the expected broadening. Neither of the *FWHM* of the two Gaussians display clear rotational modulation as, e.g., the radial velocities do. The only significant signature is that when the *FWHM* of the main emission increases the corresponding value for the absorption-reversal decreases. The seasonal mean profile, on the other hand, stays remarkably stable over time.

3.1. Mean-profile FWHM values

Table 2 lists the individual *FWHM* (in Å) of the Hα emission from the two-Gaussian fits. The seasonal *FWHM* values of the mean profiles are 3.6 ± 0.32(rms) Å in 1996, 3.6 ± 0.32(rms) Å in 1997, 3.5 ± 0.31(rms) Å in 1998, and 3.5 ± 0.31(rms) Å in 2000. These values exceed the rotational broadening by a factor of about 1.5. The rotational period and the projected rotational velocity give a minimum radius of $R \sin i = 6.3\ R_\odot$. Above *FWHM* values would then suggest an origin of at least part of the emission at an extended radius, e.g. due to a circumstellar environment of up to 1.4 $R_\star$ (assuming corotation). This would mean that the overall Hα emission is composed of two parts: a chromospheric component and a circumstellar component. This has been seen in several active stars, e.g. Oliveira & Foing (1999), who studied hydrogen and helium line profiles of the G-giant FK Com which exhibits a similar strength of chromospheric activity as UZ Lib. They also found evidence for an extended circumstellar environment up to 1.5 $R_\star$ along with a stellar absorption shell. Because the

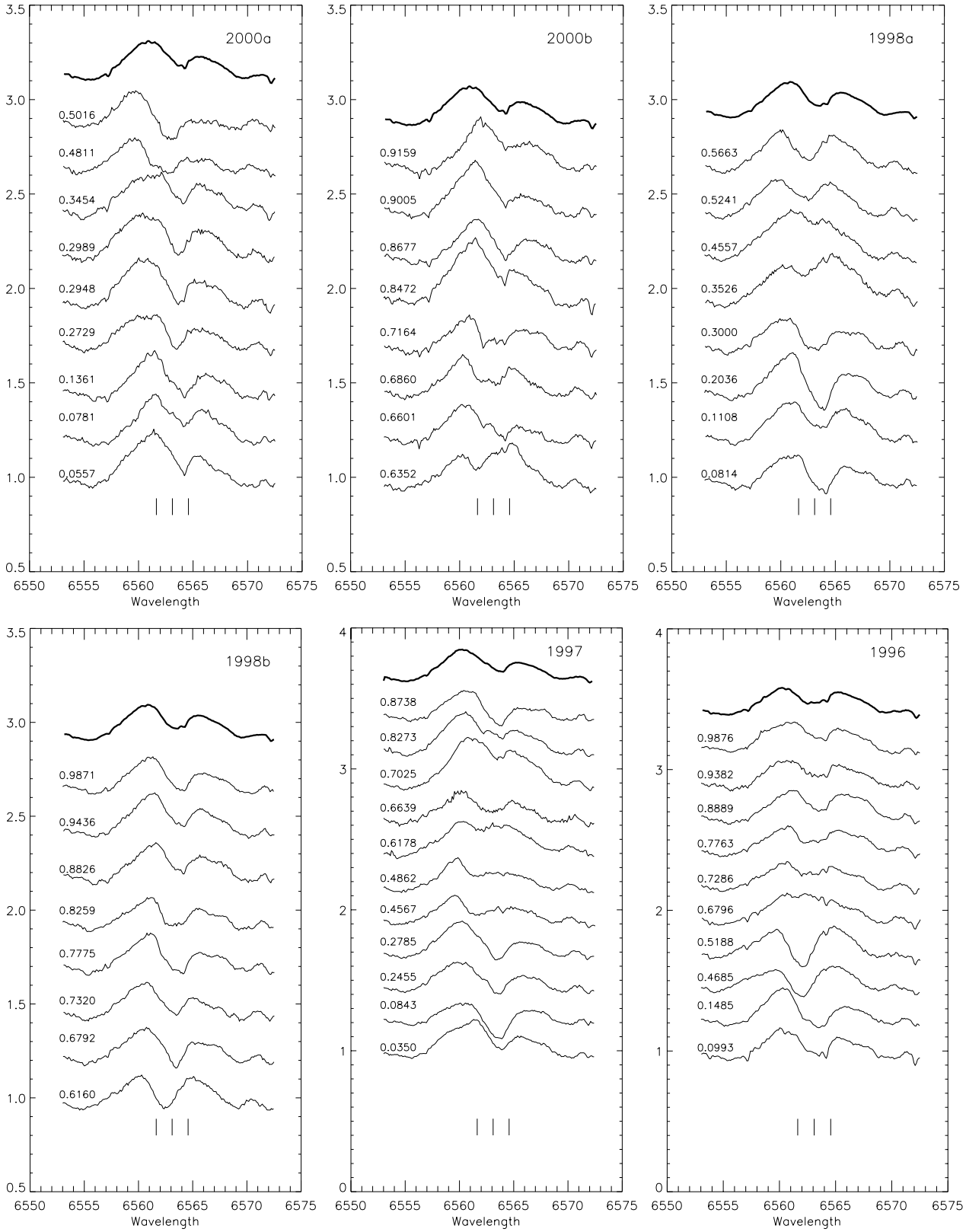

Fig. 1. The Hα-flux profiles as a function of rotational phase (arbitrarily shifted) for the observing runs 2000a, 2000b, 1998a, 1998b, 1997 and 1996. The top profile in each panel (thick line) is the seasonal average. The two 1998 sub-sets represent consecutive nights while there is a gap of 16 days between the two sub-sets for the season 2000. Notice that many phases have water-vapour lines in the spectra, which were used as accurate wavelength markers. The central Hα wavelength as well as the $\pm v \sin i$ limits are indicated.

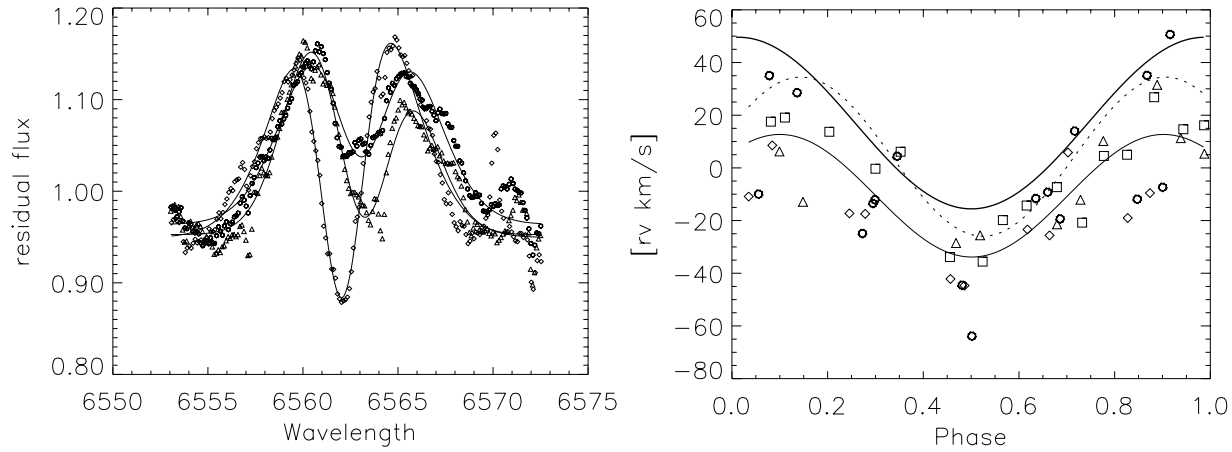

Fig. 2. *Left*: a typical two-Gaussian fit to the Hα emission component and the central absorption reversal for three phases in 1996. Triangles correspond to phase 0.1, diamonds to phase 0.52, and open circles to phase 0.77. *Right*: the radial velocities from the main emission component for all data. Triangles correspond to season 1996, diamonds to 1997, squares to 1998, and open circles to 2000. The thin line is a sinusoidal fit to all data. Superimposed are the photospheric radial velocity curve from Fekel et al. (1999) (shown as a thick line) and the fit of the radial velocities derived from the Hα absorption self-reversal (dotted line).

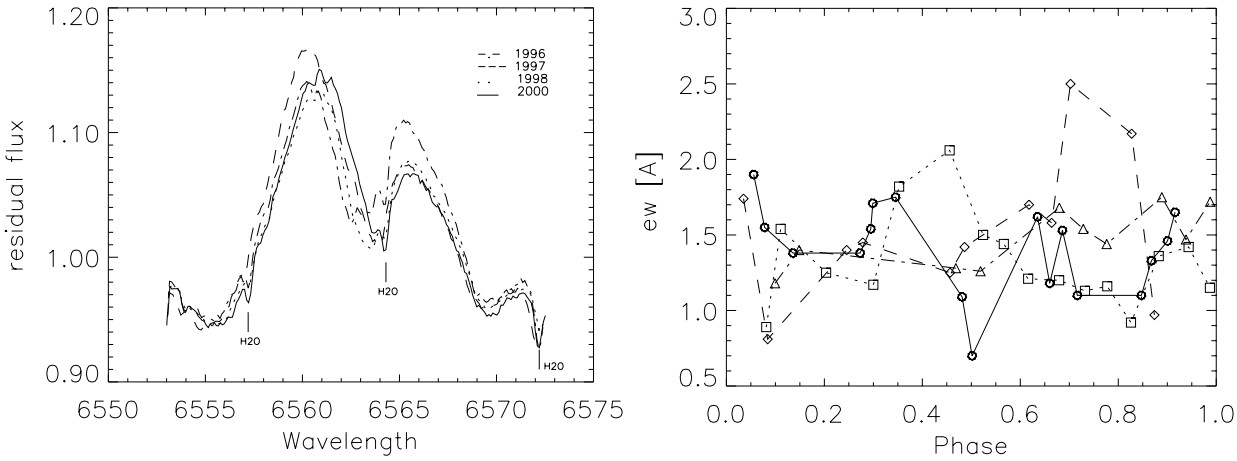

Fig. 3. *Left*: the seasonally averaged Hα line profiles. *Right*: the equivalent widths from the Hα emission. Triangles correspond to season 1996, diamonds to 1997, squares to 1998, and open circles to 2000.

FWHM of the main emission component of UZ Lib is variable, the individual profiles must be considered as formed in a non-static manner, while the seasonal profiles can be treated in a classical static approach. Consequently, future detailed modelling of individual profiles should confirm or rule out the idea of stellar absorption shells.

3.2. Hα-emission rotational modulation: Link to spots?

Oláh et al. (2002b) presented an extensive Doppler-imaging study of the UZ Lib system. Their study employed the same spectra as in the present paper but for other wavelengths as well as another additional season of data (1994), and were supplemented by simultaneous photometry. Besides the existence of a large cool polar spot with several appendages, they found two equatorial active regions that persistently appeared in the direction towards and opposite the (unseen) companion star, at average longitudes of 86° and 274°, respectively. The Hα-emission equivalent width in Fig. 3 indicates complex variations being masked with some sudden emission events which may be linked to the polar regions always in view.

The main emission component (Fig. 3, left panel) is asymmetric which suggests intense long-lived mass motions at the upper chromosphere, giving some support to the description of an active binary system with mass motions. There is rotational modulation of the main emission component (Fig. 2, right panel) which appears systematically blue-shifted by $\sim$30 km s^{-1} with respect to the photospheric lines. The latter should not be affected by chromospheric activity processes. The red wing of the Hα profile is more variable and is suppressed (according to its *FWHM*), thus providing the explanation for the blue shift of the main emission component, and suggesting intense and complex activity. Some other features as prominences, flares, ancillary magnetic field anchors etc. can not be ruled out from our data.

Due to the bound rotation of the K0 giant the hydrogen emission could also be related to the orbital motion rather then to the stellar rotation. Again, Fig. 3 demonstrates several

Table 2. Parameters from two-Gaussian Hα fitting for the seasons 1996, 1997, 1998 and 2000 from top to bottom, respectively. The indices indicate the respective Gaussian.

Phase	λ_1 (−6500 Å)	$FWHM_1$ (Å)	λ_2 (−6500 Å)	$FWHM_2$ (Å)	$W_{\lambda 1}$ (Å)	$W_{\lambda 2}$ (Å)
0.0993	62.937	2.99	63.022	2.56	1.18	0.26
0.1485	62.518	3.37	63.004	1.94	1.40	0.52
0.4685	62.176	4.25	61.996	1.73	1.28	0.38
0.5188	62.240	3.94	62.064	1.69	1.26	0.55
0.6796	62.331	4.50	...	...	1.68	0.00
0.7286	62.535	3.58	62.681	2.17	1.54	0.16
0.7763	63.023	3.85	63.058	2.23	1.44	0.22
0.8889	63.490	3.50	63.529	2.27	1.75	0.22
0.9382	63.047	3.17	63.135	2.55	1.47	0.17
0.9876	62.918	3.54	63.185	2.31	1.72	0.16
0.0350	62.562	4.29	63.594	1.55	1.74	0.18
0.0843	62.987	3.93	63.395	1.96	0.81	0.53
0.2455	62.422	3.89	63.014	2.36	1.40	0.37
0.2785	62.418	3.63	63.006	2.36	1.45	0.41
0.4567	61.877	3.08	61.951	2.69	1.25	0.23
0.4862	61.822	3.67	62.120	2.06	1.42	0.11
0.6178	62.288	3.56	62.362	2.05	1.70	0.03
0.6639	62.239	3.31	62.513	2.25	1.58	0.22
0.7025	62.928	3.37	63.200	2.30	2.50	0.10
0.8273	62.384	3.59	62.771	2.30	2.17	0.22
0.8738	62.591	3.50	63.285	2.00	0.97	0.28
0.0814	63.184	3.40	63.577	2.00	0.89	0.29
0.1108	63.218	3.27	63.328	2.46	1.54	0.26
0.2036	63.100	3.39	63.480	2.04	1.25	0.37
0.3000	62.793	3.29	62.959	2.55	1.17	0.25
0.3526	62.934	3.95	62.515	2.09	1.82	0.07
0.4557	62.059	4.25	62.784	1.23	2.06	0.03
0.5241	62.021	3.28	62.092	2.40	1.50	0.19
0.5663	62.366	3.52	62.424	2.09	1.44	0.30
0.6160	62.487	3.74	62.510	1.76	1.21	0.33
0.6792	62.640	3.96	63.256	1.68	1.20	0.22
0.7320	62.345	3.41	62.915	1.89	1.13	0.21
0.7775	62.899	3.48	63.400	1.99	1.16	0.27
0.8259	62.909	3.34	63.250	1.87	0.92	0.23
0.8826	63.387	3.34	63.685	2.02	1.36	0.19
0.9436	63.121	3.43	63.558	1.92	1.42	0.26
0.9871	63.154	3.18	63.495	2.16	1.15	0.18
0.0557	62.582	3.93	63.678	1.50	1.90	0.14
0.0781	63.567	2.90	63.689	2.35	1.55	0.18
0.1361	63.425	2.96	63.653	2.33	1.38	0.28
0.2729	62.255	4.45	63.403	1.25	1.38	0.19
0.2948	62.505	3.95	63.295	1.94	1.54	0.19
0.2989	62.535	4.60	63.440	1.73	1.71	0.21
0.3454	62.897	4.88	63.788	1.37	1.75	0.20
0.4811	61.825	2.96	62.010	2.54	1.09	0.26
0.5016	61.402	3.09	62.339	2.01	0.70	0.34
0.6352	62.546	3.50	62.178	1.98	1.62	0.10
0.6601	62.598	2.93	62.785	2.60	1.18	0.16
0.6860	62.376	2.81	62.489	2.24	1.53	0.20
0.7164	63.106	3.02	63.173	2.60	1.10	0.21
0.8472	62.540	3.72	63.464	1.66	1.10	0.09
0.8677	63.569	3.17	63.949	2.07	1.33	0.25
0.9005	62.639	3.61	63.771	1.78	1.46	0.19
0.9159	63.909	2.90	64.127	2.28	1.65	0.08

kinds of variability including sudden emission events. During 1997 there are short-term, systematic increases of the hydrogen emission on time scales much below the rotational period. This might be expected and associated with some kind of low-energetic flaring. Practically the same magnitude of sudden variability is recognized in season 1998, but this time a systematic decrease of the emission was seen, and at a different phase. An explanation with flares is supported by many other results, most recently by Gondoin (2003). Using XMM-Newton during 2000/2001, he demonstrated the existence of bremsstrahlung emission from plasma at high temperature (3×10^7 K).

4. Model computations

The coupled equations of radiative transfer, statistical equilibrium, and hydrostatic equilibrium were solved for plane-parallel and spherical geometries using the Pandora code (Avrett & Loeser 2002), both with complete redistribution and partial redistributin of line radiation. The rate equations include bound-bound and bound-free radiative and collisional rates, and processes such as de-electronic recombination. A combination of simultaneous and iterative methods were used to solve the coupled equations of radiative transfer and statistical equilibrium for lines and continua. The overall maximal relative change of all model quantities and level populations in each final iterative solution was 0.01 at every depth point. We used an 8-level hydrogen atom after concluding that a 15-level calculation did not justify the longer CPU running time.

The photospheric structure was taken from the radiative equilibrium models of Kurucz (1992 and private communication) for a star of effective temperature $T_{\rm eff} = 4800$ K, a metallicity of either [M/H] = −1 or [M/H] = −0.6, and a surface gravity of $\log g = 2.5$. Starting at the photospheric temperature of 4000 K, chromospheric and transition-region structures were added, extending outward to a final temperature of 10^6 K. The approach is similar to that of Jordan et al. (1987) and Linsky et al. (2001) who demonstrated for a number of G and K stars the basic properties of upper atmospheres and the energy balance, based on an emission measure analysis of strong UV spectral lines.

The atmospheric depth variable we use is $\log \mathrm{DM}$ or the log of the mass column density. The chromospheric temperature rise starts at 4000 K where $\log \mathrm{DM} = 1.01$ and 0.89 for [M/H] = −1 and −0.6, respectively. The chromospheric distribution is linear in $\log T$ vs. $\log \mathrm{DM}$ extending to the coordinate $\log T = T2$, $\log \mathrm{DM} = \mathrm{M2}$. From there, the transition-region distribution extends linearly to $\log T = 6$, $\log \mathrm{DM} = \mathrm{M3}$.

We show results for 32 emission-line chromospheres (13 for [M/H] = −0.6 and the rest reflecting [M/H] = −1 and various physical inputs like sphericity, non-standard outer non-linear variations – models 5 and 6 in particular; etc.) that provide approximate upper and lower bounds compared with the observed profiles. Figures 5a and 5b show the temperature distributions and the flux profiles for [M/H] = −1. Table 3 lists the values of M3, M2, and $T2$ ($T2 = T\mathrm{C}$ the temperature at the top of the chromosphere) for each model and the calculated peak and central residual fluxes.

The partial frequency redistribution (PRD) approximation introduces the effects of monochromatic scattering in the line wings, whereas complete frequency redistribution (CRD) assumes that a photon absorbed in the wings is likely to be re-emitted near line center. We assumed PRD in our calculation of the H-alpha profiles, which had little effect on the central and peak values, but reduced the flux in the line wings beyond the peaks, quickly approaching the continuum value, in better agreement with the observed line shape than in the case of CRD.

The results shown in Figs. 5a and 5b and in Table 3 were obtained from plane-parallel calculations for simplicity. Spherical calculations with a stellar radius 6 and 3 times solar typically give flux profiles with peak and central values enhanced by factors about 1.15 and 1.25, respectively.

We found that profiles computed in LTE are totally unrealistic, giving orders-of-magnitude larger emission, and no central reversals.

The calculations also used a turbulent velocity distribution, assumed to be 3 km s^{-1} in the photosphere, 10 km s^{-1} in the transition region, and varying linearly with log DM in between. The Doppler broadening of hydrogen lines is mostly thermal so that this additional broadening is of secondary importance. These values also add a turbulent pressure in the hydrostatic equilibrium equations, but again the effect is secondary.

Another active sub-giant star (II Peg) was studied in a similar way by Short et al. (1998), but in plane-parallel geometry. The authors specifically modelled Hα, Hβ, Hγ, Hδ and the Ca II spectra but also had to restrict their fits to line-wing comparisons as far as the hydrogen-alpha profile is concerned. Clearly, their calculated absorption self-reversal is not in agreement with the observed one. On the other hand they nicely succeeded in reconstructing the Hα/Hβ total emission ratio without a recourse to extra-atmospheric material.

4.1. Lyman-lines balance and level populations

If a radiative transition is in detailed balance, the net radiative rate in the line is zero. Detailed balance assumes large optical thickness so that the line radiation field is locally in equilibrium with the level population and the non-local radiative transfer effects are negligible. There have been numerous discussions indicating that the solar Lyman lines are in detailed balance at depths where the Balmer lines are formed. Given the model atmosphere the levels up to 2 may be affected but at the optical depths ~0.1 for the Lyman continuum the effect to level populations may also come from the (log) column mass points <−5 (e.g. Milkey & Mihalas 1973). We considered the computations in both detailed balance and with properly recomputed radiative rates but the gross effect on the hydrogen alpha transition is very small.

The ionization ratio as well as the level departure coefficients indicate that only the first level is strongly controlled by ionizing radiation from the transition region (log DM ≈ −3). The higher level departure coefficients are determined by conditions in the lower chromosphere. The departure coefficients are larger than unity also starting from the lower chromosphere,

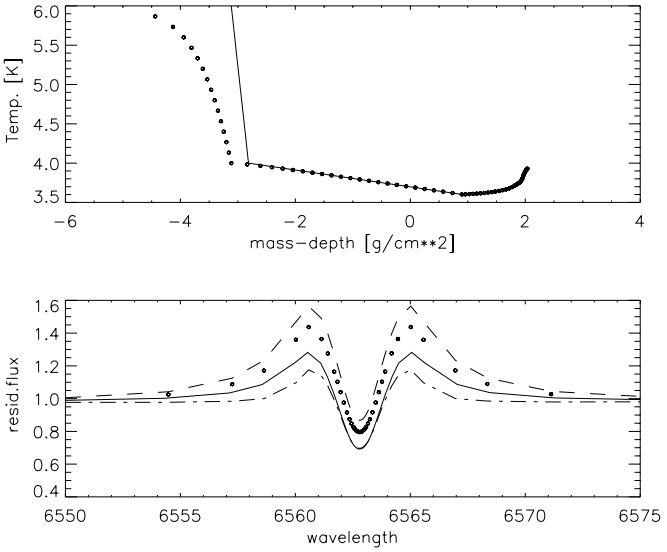

Fig. 4. The effect of physical inputs in modelling. The model 4 (solid line) and 7 (dash dot line) stand for the complete redistribution (CRD) vs. PRD in plane-parallel mode and model 5 dots and model 6 (dashed line) stand for stellar radius 6 $R_\odot$ vs. 3 $R_\odot$ in spherical mode and CRD option.

reflecting population/depopulation processes. The largest effect is again for the first hydrogen level.

4.2. Metallicity

We have devoted considerable effort to understanding how the variability of the star and its chromospheric activity influences the hydrogen alpha profile, but an abundance analysis is also needed. We derived a preliminary metallicity from several transitions in the region 6330–6650 Å, but heavy blending is present as a result of the high value of $v \sin i$. Consequently, we adopted the values responsible for velocity fields from Strassmeier (1996). Afterwards, some reference transitions were adopted for the first iteration, namely Ca I 6439.08, Fe I 6401.00, Fe I 6411.66, Fe I 6393.60 and Fe I 6609.11 Å.

Having determined the abundances we included further single or simply blended transitions (Ca I 6343.3, Fe I 6344.15, Fe I 6421.35, Fe I + Ca I 6462.71, Fe I + Ti I 6456 and Fe I 6593.4 Å). A more advanced abundance analysis, i.e. including more transitions and a careful deblending due to $v \sin i$ along with molecular identifications is, however, beyond the scope of this paper.

The average metallicities are −0.7±0.02 for Fe, and −0.35± 0.02 for Ca from the ATLAS9 model, and −0.90 ± 0.03 and −0.51 ± 0.03, respectively for the PHOENIX model (version 10.8.8, Allard & Hauschildt 1995). The overall metallicity [M/H] is −0.53 and −0.71 from the two atmospheric codes, respectively. The ~0.18 dex difference from the models is still in the range of the errors quoted in spectroscopic abundance analyses but the differences in the temperature-pressure diagram give the clue (effect of various opacities, atomic data, input physics like LTE vs. NLTE, geometry etc.).

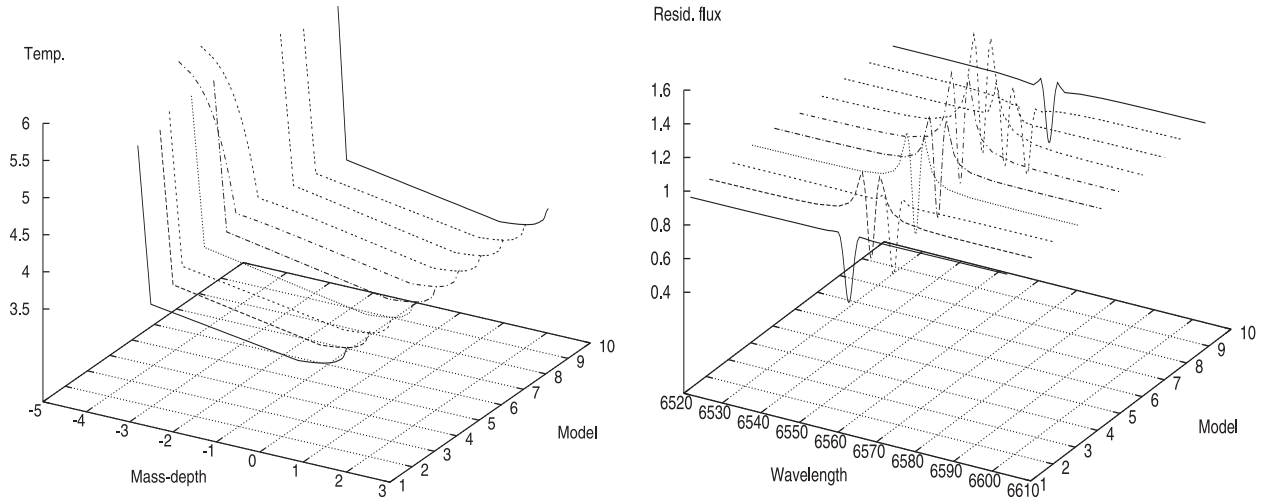

Fig. 5. a) A sample of models and **b)** corresponding hydrogen line profiles. See Table 3 for detailed model description.

4.3. Age and H-R position

There seems to be an inconsistency (in luminosity and radius for example) with regard to the distance on the one hand and stellar radius, size of the orbit, and the inclination of the rotational axis on the other hand (Oláh et al. 2002a). This arises due to the large Hipparcos parallax and considerations of the stellar parameters as derived from radial velocities, Doppler imaging, and the light curve. Supposing the effective temperature of the K0 primary, its radius of $R \approx 6{-}8\ R_{\odot}$, and the mass function are derived satisfactorily, this suggests a primary mass of around $1.5{-}2.0\ M_{\odot}$ (Oláh et al. 2002b).

The chromospheric modelling is not directly relevant to constrain evolutionary models, particularly if the rotation rate is controlled by tidal effects in a binary rather than by age-related breaking but to achieve global picture of target, the evolutionary status and the position on HR diagram are worth mentioning. Some realistic results can be achieved using the post-main-sequence evolutionary models of Schaller et al. (1992). They computed models with overshooting for solar and sub-solar metallicities, various mixing-length ratios, and core-burning fragmentation (H, He burning etc.). Using their models it is indicated that the primary of UZ Librae is at an age of $\approx 5.0 \times 10^8$ yr if still in the H-burning phase. The H-burning phase is counted from the zero-age main sequence until central H-exhaustion. The lifetime scale is offered also for the He-burning phase (i.e. He fragment is burnt during main H burning phase) with the counting from the stage when two thousands of helium (in mass fraction) has been burnt to central He-exhaustion. The time scale for He-burning is $\approx 1.0 \times 10^8$ yr. In fact, the metallicity plays a negligible role here. It is beyond the limit of these evolutionary models to trace the secondary.

5. Conclusions

This work is the attempt to study the upper part of the atmosphere (chromosphere and transition region) of an active K0 giant with (unseen) companion. Based on the study of the radiation field via the hydrogen alpha transition by means of conventional 1D-static modelling of the seasonal mean profiles as a first step, we arrived at the following results:

1. The best approximation to the Hα profile was obtained with the chromospheric rise starting at log DM (logarithmic column mass) equal to 0.9 and the upper chromosphere ending at log DM ≈ -1.8 with a temperature of $\approx$7400 K.
2. The transition region/coronae ends at the temperature of about 100 000 K extending almost linearly to that value corresponding to log DM $= -6$.
3. Evidence for circumstellar matter or at least a global velocity field in form of an absorption shell comes, firstly, from the Hα *FWHM* that exceeds the $v \sin i$ value by almost a factor two, secondly, the existence of a variable central absorption self-reversal and, thirdly, by a persistent asymmetry of the Hα-emission profile, extending out to perhaps $1.5\ R_{\star}$.
4. Two-Gaussian fitting of the Hα-line profile suggests a variable velocity field; the radial velocities of the hydrogen emission display rotational modulation.
5. The hydrogen emission equivalent width (as derived from the numerical integration of the Gaussian fits) possibly displays rotational modulation as well as several sudden flare-like events at discrete phases.
6. The more dramatic changes of the line profiles occur mainly in the red line wing, suggesting down-flow events at its formation height.
7. A comparison with evolutionary models suggest inconsistencies of basic parameters such as luminosity and age, and may be interpreted as evidence for additional processes linked to atmospheric mass motions, a circumstellar absorption shell, mass transfer, and chromospheric activity of the main K0 component. The complex properties of binary and heterogeneous chromosphere properties in particular can not be fully disentangled by seasonal profiles study.
8. Finally, our preliminary metallicity of the system is sub-solar, [M/H] ≈ -0.5 from a comparison with ATLAS9 models or -0.7 from a comparison with PHOENIX models.

These conclusions support a picture of chromospheric activity of the primary together with extra absorption in form of

Table 3. A set of models and (original) peak and central line fluxes.

No.	M3	*T*C, M2	Peak	Cen. Res.	Note
1	−2.8	3.990, −2.5	none	0.50	pp, CRD, −0.6
2	”	3.954, −2.5	1.39	0.62	pp, CRD, −0.6
3	−3	3.954, −2.7	1.08	0.39	pp, CRD, −1
4	”	4.000, −2.7	1.49	0.47	pp, CRD, −1
5	−4.5	4.000, −3.1	1.70	0.55	6 $R_\odot$, CRD, −1
6	”	” , ”	1.86	0.60	3 $R_\odot$, CRD, −1
7	−3.0	4.000, −2.7	1.48	0.47	pp, PRD, −1
8	−3.0	3.954, −2.7	1.05	0.39	pp, PRD, −1
9	−2.7	3.954, −2.5	1.15	0.48	pp, PRD, −1
10	−2.6	3.954, −2.4	1.21	0.54	pp, PRD, −1
11	−2.4	3.954, −2.2	1.38	0.67	pp, PRD, −1
12	−2.2	3.954, −2.0	1.59	0.82	pp, PRD, −1
13	−2.2	3.903, −2.0	1.05	0.66	pp, PRD, −1
14	−2.0	3.903, −1.8	1.22	0.80	pp, PRD, −1
15	−1.9	3.903, −1.8	1.25	0.85	pp, PRD, −1
16	−1.8	3.903, −1.7	1.36	0.94	pp, PRD, −1
17	−1.8	3.845, −1.7	1.15	0.83	pp, PRD, −1
18	−1.7	3.845, −1.6	1.25	0.92	pp, PRD, −1
19	−1.6	3.845, −1.5	1.36	1.01	pp, PRD, −1
20	−3.0	4.000, −2.7	2.05	0.74	pp, PRD, −0.6
21	−3.0	3.954, −2.7	1.28	0.57	pp, PRD, −0.6
22	−2.7	3.954, −2.5	1.50	0.74	pp, PRD, −0.6
23	−2.6	3.954, −2.4	1.63	0.84	pp, PRD, −0.6
24	−2.4	3.954, −2.2	1.93	1.04	pp, PRD, −0.6
25	−2.2	3.954, −2.0	2.29	1.28	pp, PRD, −0.6
26	−2.2	3.903, −2.0	1.47	0.99	pp, PRD, −0.6
27	−2.0	3.903, −1.8	1.76	1.21	pp, PRD, −0.6
28	−1.9	3.903, −1.8	1.83	1.29	pp, PRD, −0.6
29	−1.8	3.903, −1.7	1.99	1.43	pp, PRD, −0.6
30	−1.8	3.845, −1.7	1.70	1.26	pp, PRD, −0.6
31	−1.7	3.845, −1.6	1.86	1.39	pp, PRD, −0.6
32	−1.6	3.845, −1.5	2.00	1.52	pp, PRD, −0.6

The abbreviations in note section: [M/H] – metallicity, pp – plane-parallel mode, CRD – complete redistribution and PRD – partial frequency redistribution.

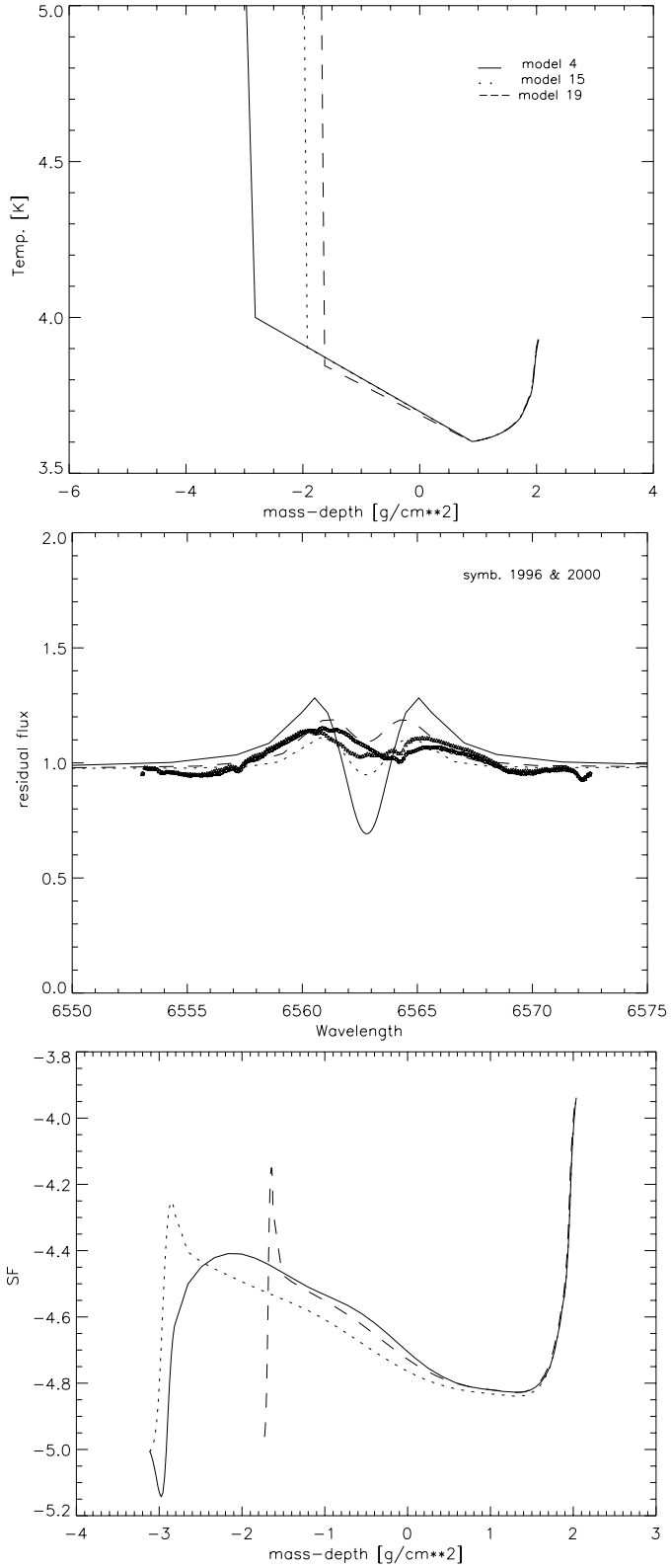

Fig. 6. Results from modelling the mean Hα profiles of UZ Librae. *Top panel*: atmospheric temperature versus mass-depth on a logarithmic scale; models Nos. 4, 15 and 19 as described in the text, *middle*: line profiles corresponding to the models in above panel, *bottom*: total line source functions (SF) in units of (erg s^{-1} cm^{-2} Å^{-1}).

a circumstellar shell (possibly stable prominences). However, atmospheric modelling at this stage can not distinguish between a stellar radius of 3 or 6−8 $R_\odot$, as obvious from the discrepancy due to the surprisingly large Hipparcos parallax, instead plane-parallel mode is suitable as a first step in modelling. We intend to follow-up this study with a more detailed study of the effects of surface flow velocities and with overall energy distribution including the individual IUE satellite emission features in spectra as well. The rotational modulation of the Hα profile is remarkable for an active star, and this deserves special consideration of *both* radiation and velocity fields as well as other solar-type phenomena, such as spiculae-like velocity outflows and inflows.

Acknowledgements. K.G.S. and M.Z. acknowledge the support of the Deutsche Forschungsgemeinschaft from DFG-grant STR645/1. We are grateful to R. Loeser for assistance with the atmospheric modelling calculations. We also thank to anonymous referee for many helpful comments.

References

Allard, F., & Hauschildt, P. H. 1995, ApJ, 445, 433
Avrett, E. H., & Loeser, R. 2003, IAU Symp. 210, ASP Conf. Ser., in press
Bopp, B. W., & Stencel, R. R. 1981, ApJ, 247, L134
Eriksson, K., Linsky, J. L., & Simon, T. 1983, ApJ, 272, 665
Fekel, F. C., Strassmeier, K. G., Weber, M., & Washuettl, A. 1999, A&AS, 137, 369
Fontenla, J. M., Avrett, E. H., & Loeser, R. 2000, ApJ, 572, 636
Grewing, M., Bianchi, L., & Garrido, R. 1989, A&A, 223, 172
Giampapa, M. S., Worden, S. P., & Linsky, J. L. 1982, ApJ, 258, 740
Gondoin, P. 2003, A&A, 400, 249
Houdebine, E. R., & Panagi, P. M. 1990, A&A, 231, 459
Houdebine, E. R. 1996, IAU Symp. 176, ed. K. G. Strassmeier, & J. L. Linsky (Dordrecht: Kluwer), 547
Jordan, C., Ayers, T. R., Brown, A., Linsky, J. L., & Simon, T. 1987, MNRAS, 225, 903
Kurucz, R. L. 1992, Rev. Mex. Astron. Astrofis., 23, 45
Linsky, J. L., Redfield, S., Ayres, T. R., Brown, A., & Harper, G. 2001, ASP Conf. Ser., 242, 247
Milkey, R. W., & Mihalas, D. 1973, ApJ, 185, 709
Oláh, K., Jurcsik, J., & Strassmeier, K. G. 2003, A&A, 410, 685
Oláh, K., Strassmeier, K. G., & Granzer, T. 2002a, AN, 323, 453
Oláh, K., Strassmeier, K. G., & Weber, M. 2002b, A&A, 389, 202
Oliveira, J. M., & Foing, B. H. 1999, A&A, 343, 213
Rice, J., & Strassmeier, K. G. 2000, A&AS, 147, 151
Schaller, G., Schaerer, D., Meynet, G., & Maeder, A. 1992, A&AS, 96, 269
Schrijver, C. J. 2002, AN, 323, 157
Short, C. I., Byrne, P. B., & Panagi, P. M. 1998, A&A, 338, 191
Strassmeier, K. G. 1996, A&A, 314, 558
Vernazza, J. E., Avrett, E. H., & Loeser, R. 1973, ApJ, 184, 605
Vernazza, J. E., Avrett, E. H., & Loeser, R. 1981, ApJS, 45, 635